NONLINEARITIES OF SHORT AND LONG WAVES ACROSS THE SHOALING, SURF AND SWASH ZONES: PHYSICAL MODEL RESULTS

Mariana V.L. Rocha[1,2], Hervé Michallet[1], Paulo A. Silva[2], Tiago Abreu[3], Eric Barthélemy[1]

Abstract

In the scope of GLOBEX HYDRALAB IV project, laboratory experiments were performed in a 110-m-long beach, with a 1/80 rigid-bottom slope. With the free-surface elevation and cross-shore velocity data, the evolution of velocity nonlinearities along the profile (shoaling, surf and swash zones) is analyzed, both for short and long waves. To better investigate the different hydrodynamic processes at work, the third-order velocity moment terms are computed, and their relative importance along the profile is evaluated, relative to breakpoint position. Short-wave skewness, short-wave variance correlation to long-wave velocity and stirring by short waves and transport by mean flow were found to be the dominant terms outside the surf zone. Inside the surf zone, stirring by both short and long waves and subsequent transport offshore by the mean flow, and skewness of short waves were found to be the main driving mechanisms. In the swash zone, where long waves dominate, the third-order velocity moment terms tend to assume positive values. A thorough analysis of swash zone data processing and hydrodynamics is carried out and some of the current limitations of such processing are unraveled.

Key words: physical model, random waves, cross-shore profile, skewness, asymmetry, swash zone.

1. Introduction

Understanding nearshore morphodynamics implies a profound knowledge of the hydrodynamics and the complex interaction between motions at different spatial and temporal scales.

The cross-shore beach profile is one of the most important characteristics of natural sea coasts, as it can be used to evaluate the accretion or erosion of a specific coastal site, as well as the vulnerability of particular regions (Didenkulova and Soomere, 2011). Along this cross-shore profile, as the surface gravity waves propagate from deeper waters to the shore, their shape changes, primarily due to nonlinear wave interactions (Elgar and Guza, 1985; Doering and Bowen, 1995) and further on due to breaking (Michallet *et al.*, 2011). The nonlinear effects amplify the higher harmonics and cause the oscillatory flow to transform from sinusoidal in deep water, through velocity-skewed in the shoaling zone, to velocity-asymmetric in the inner surf and swash zones. Skewness and asymmetry influence on sediment transport is hard to study, because it is difficult to isolate those phenomena from other breaking phenomena (Ruessink *et al.*, 2011). However, these nonlinearities are of paramount importance for understanding sediment dynamics.

In addition to short-wave nonlinearities, the presence of long waves and wave groups also results in an additional wave-induced velocity and influences the short-wave hydrodynamics and larger scale processes, such as the formation of standing waves or a cross-shore and longshore nodal structure both inside and outside the surf zone (Baldock *et al.*, 2011). Further, long waves can themselves contribute to velocity skewness and asymmetry at low frequencies, particularly for very dissipative mild-slope beach profiles ($\beta_b < 0.1$), where long-wave shoaling and breaking can also occur (van Dongeren *et al.*, 2007; de Bakker *et al.*, 2013).

The influence of all these processes on water motion and sediment transport varies significantly along the cross-shore beach profile, and it is the understanding of these relative contributions that is of paramount importance to better grasp how is nearshore morphodynamics driven.

The swash zone is the limit between the aerial and the submerged beach areas which is intermittently covered and exposed by wave action (Alsina and Cáceres, 2011). In this zone, particularly for very dissipative beaches, high infragravity-energy levels, saturation and dissipation of short-wave energy in the surf zone and saturation of bore-driven swash oscillations at short-wave frequencies contribute for a

[1]LEGI, CNRS/G-INP/UJF, BP53, 38041 Grenoble, France. m.rocha@ua.pt, herve.michallet@legi.grenoble-inp.fr,eric.barthelemy@grenoble-inp.fr.
[2]CESAM, University of Aveiro, Campus de Santiago, 3810-193 Aveiro, Portugal. psilva@ua.pt
[3]CESAM, Polytechnic Institute of Viseu, Campus Politécnico, 3504-510 Viseu, Portugal. tabreu@estv.ipv.pt

dominance of long-wave motion. Aagaard and Hughes (2006) define three areas in the swash zone depending on their submergence ratio. The lower swash zone corresponds to an immersion during 75 to 95 % of the measuring time, the mid swash presents periods of submergence between 40 and 75 % and the upper swash is where the beach is only 1 to 40 % of the measuring time covered by water. Across these areas and the inner-surf zone, different "forcing" phenomena are considered by Cáceres and Alsina (2012) as sediment transport controlling mechanisms, namely wave breaking and bore collapsing, backwash, sediment advection, infiltration/exfiltration effects, fluid velocity asymmetries, long waves and wave groups and acceleration asymmetry in the cross-shore flows.

During the last ten years important progress has been made in the understanding of swash dynamics and a great part of the scientific community involved in studying the beach profile hydrodynamics and morphodynamics has turned its attention to this particular zone of the beach. Nevertheless, many uncertainties remain on the hydrodynamic processes acting within the swash zone. High-resolution in space and time data sets can, ultimately, help shedding some light on this subject.

Therefore, the present work is based on physical model results and aims improving the current knowledge of cross-shore hydrodynamic processes that influence sediment transport along the beach profile, spanning from the shoaling zone, through the surf zone onto the swash zone. Thereunto, following the work of Guza and Thornton (1985) and Russell and Huntley (1999) and the approach of Mariño-Tapia *et al.* (2007), the variation of the normalized cross-shore velocity moments along the profile relative to the breakpoint position is analyzed to better comprehend the relative contributions of incident waves, long period motions, mean flows and interactions between them. Since few studies before have focused on trying to describe the velocity nonlinearities (skewness and asymmetry) in the swash zone, a greater emphasis is put on this attempt, and detailed description of swash zone data processing is presented.

2. Experimental Set-up

The data used in this work were collected on the scope of GLOBEX (Gently sLOping Beach Experiments) Hydralab IV project, which aimed improving the understanding of nonlinear water motion on gently-sloping beaches and was held during the months of March and April 2012, in the Scheldegoot at Deltares, in Delft. A detailed overview of these experiments is done by Ruessink *et al.* (2013).

The flume had a fixed bed and was 110-m long and 1-m wide, with an initial plain section of 16.57 m, and a slope of 1/80 until the end of the flume. The mean shoreline was located at 84.57 m from the wave maker (x = 0), corresponding to a mean water depth above the plain section of 0.85 m.

During the experiments three different types of wave conditions were simulated, but this work focuses on the three random-wave cases based on the JONSWAP spectrum (series A), for being the most closely related to the wave conditions found in nature (Table 1).

Table 1. Random wave conditions.

Condition	H_s (m)	T_p (s)	γ	Prototype
A1	0.10	1.60	3.3	H_s = 2 m; T_p = 7 s
A2	0.20	2.25	3.3	H_s = 4 m; T_p = 10 s
A3	0.10	2.25	20	H_s = 2 m; T_p = 10 s

A suite of instruments were deployed during all runs, including, among others, 22 wave gauges (10 resistive-type and 12 capacitive-type), 5 ElectroMagnetic Current Meters (EMCM) and 2 side-looking Acoustic Doppler Velocimeters (ADV) for recording flow velocities.

Each condition was run for 75 min with the gauges and EMCMs sampling at 128 Hz, followed by a rest period of approximately 30 min. After all conditions were completed, most instruments were repositioned and the 7 conditions were repeated with exactly the same wave-board motion. In total, 10 batches were run, resulting in a total of 190 positions with water level measurements and 47 with flow-velocity data (at 1-30 cm above the bed). An ADV, sampling at 200 Hz and positioned near the bottom (at *a.c.*6 mm above the bed), was used to extend the ECMCs velocity measurements (which ended at x = 79.48 m) further into the inner-surf/swash zone for depths shallower than 5 cm, adding 10 more cross-shore positions velocity measurements (starting at x = 78.73 m), of which at least three, in average, were located in the swash zone. Also, for the most inshore positions, the wires of the capacitive gauges were stretched to the bottom, where they were fixed, so that the lowest water level possible was

measured. The ADVs were located close to one of the flume walls (at an *a.c.*15 cm distance), while EMCMs and wave gauges were positioned along the central line of the flume.

For this work, only the measurements concerning free-surface elevation and cross-shore velocity are considered and the region of the beach profile in focus starts in the shoaling zone (at a depth about two-times the breaking depth) and extends to the end of the upper-swash zone.

3. Data processing and preliminary analysis

3.1 Time-series and energy spectra

The high-resolution in time and space time series obtained with the wave gauges and the flow meters allow a clear observation and analysis of the wave propagation across the shoaling, breaking and swash zones for both short and long waves. Figure 1 shows an example of the time series obtained for different positions along the profile, where long waves were obtained from filtering the full signal at half the peak frequency.

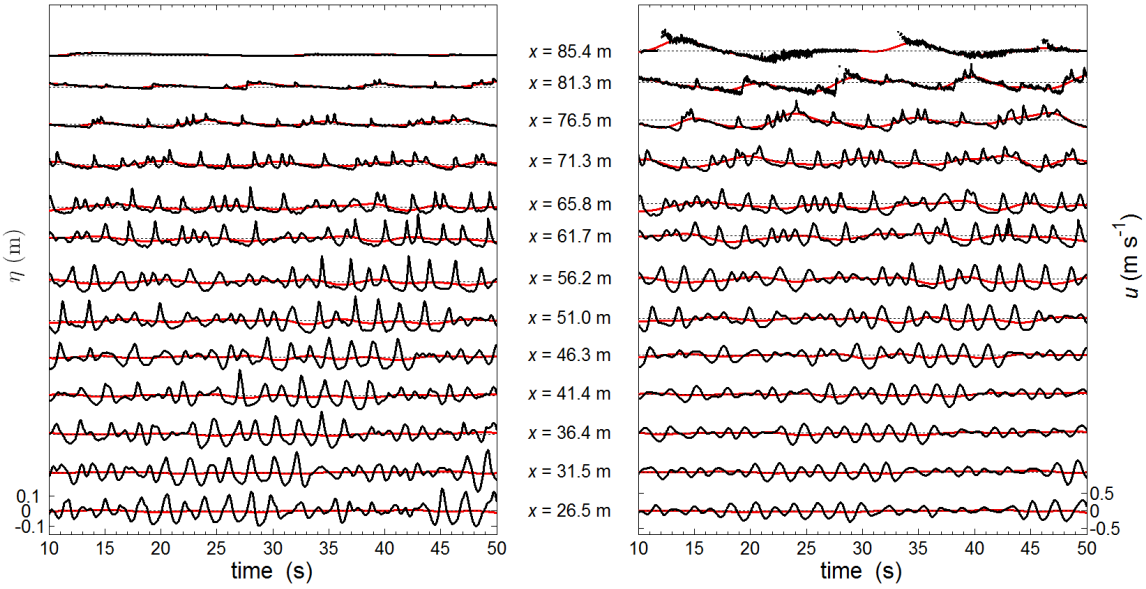

Figure 1. Example of free-surface elevation (left) and velocity (right) time series obtained for condition A2 for diverse positions along the cross-shore profile. Full signal is in black and low-pass signal in red.

Observing the short waves propagating towards the shore, it is clear their progressive shape change to skewed and asymmetric, finally capturing each other within the same wave group to propagate higher up the beach as bores, associated with the long-wave motion. The velocity plots reflect the same evolution, with velocity changing from simple orbital motion to swash events with marked uprush and downrush phases. The presence of wave groups and the clear signature of the long waves are also evident both in the free-surface and the velocity time series, progressively more marked as the waves approach the shore.

Frequency (Hz)

Figure **2** presents the velocity spectra at five distinct cross-shore positions. For such a dissipative beach as the one considered in these experiments (1/80 slope), strong infragravity motion is expected to significantly contribute for the energy spectra along the profile, in particular in the swash zone.

Analyzing the spectra, it can be seen that, for the two shoaling positions (x = 30.1 m and x = 50.7 m), energy is concentrated mostly in the high-frequency range, with a clear peak at the peak frequency of incident waves. The high-frequency end of the spectrum reveals some background noise, whereas in the low-frequency end there is also a marked peak around 0.03 Hz, corresponding to long-wave motion (de Bakker *et al.*, 2013).

For the first position after the breakpoint (x = 68.5 m), there is a strong decay of the incident-frequency component linked to a significant energy transfer to higher frequencies, with a distinct peak around

0.88 Hz (the first harmonic of the peak frequency), following a trend of f^{-3} associated with wave saturation or an inverse energy cascade.

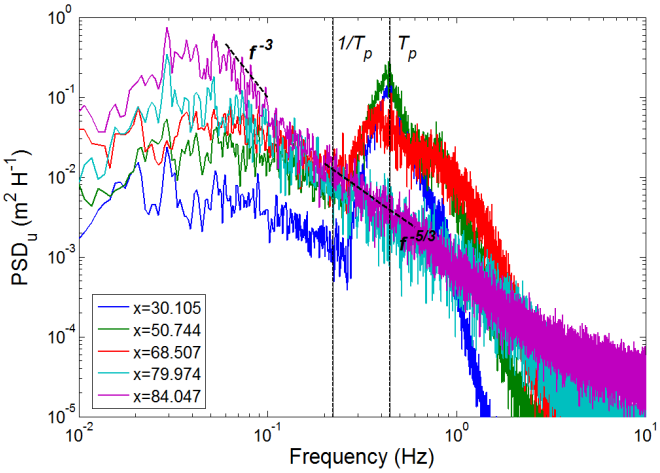

Figure 2. Cross-shore velocity spectra obtained for condition A2 at five different positions along the beach, corresponding to shoaling (blue), shoaling close to breaking (green), surf zone (red), inner-surf /lower-swash zone (cyan) and upper-swash zone (purple).

As waves propagate closer to the shore in the inner-surf/swash zone, the velocity energy levels at frequencies greater than 0.1 decrease approximately as $f^{-5/3}$, consistent with an inertial subrange, and energy is transferred to sub-harmonics, with energy levels peaking at infragravity frequencies. For the position further inshore, the low frequencies in the range of 0.04-0.08 Hz also start decaying following f^{-3}, reflecting possible saturation and breaking of infragravity waves.

Overall, these data depict the importance of long-wave motion, particularly for the swash zone, which implies the analysis and treatment of data collected in the swash zone, which is still a challenging issue.

3.2 Swash data processing

With the ADV located in the inner-surf/swash zone, 12 flow-velocity time series were obtained. Most ADV measurements were made at the lowest-position possible (centre of control volume at about 6 mm above the bed). Most time series have a 69-min duration, although some are shorter, with 22 to 33 min, varying between runs. For all series considered, the first 6 min were excluded from analysis. Depending on the wave conditions (A1, A2 or A3), measurements were performed in three to five cross-shore positions within the swash zone, spanning from the lower to the upper swash: x = 83.62 m, x = 84.29 m, x = 84.56 m, x = 85.39 m and x = 86.51 m, for a shoreline at rest located at x = 84.56 m from the wave-maker (see Figure 4).

The swash zone is, by definition, a zone which is intermittently covered by water. This means that any instrumentation positioned in this zone will be submerged during discrete periods. For water-level measurements, this only means that, at times, zero values appear within the time series. For the velocity measurements, however, it means that parts of the signal are too noisy and present unrealistic values. It is then necessary to follow a rigorous procedure in order to define which values are to be considered and which to be excluded from analysis.

The first step of swash data analysis consisted in synchronizing the cross-shore velocity time series with the free-surface elevation time series measured at the closest wave gauge. The velocity time series were then de-spiked (Mori *et al.*, 2007), as a preliminary way of eliminating spurious data points.

Voulgaris and Trowbridge (1998) have shown that accurate ADV measurements can be difficult to obtain within a 1-cm distance from walls. Hence, the purpose of the following method is to evaluate the reliability of measurements performed very close to the bed, in the swash zone.

The first criterion for controlling the output of the ADV was based on the free-surface elevation relatively to the control-volume height. However, as the wave gauges were not always at the exact cross-shore position of the ADV and also due to the occasional existence of resonant cross-modes in the transversal direction of the flume (van der A et al., 2013), the wave fronts depicted in the free-surface plots were not always exactly in phase with the sudden onshore-velocity increase associated with the uprush. Therefore, a Corr and a SNR criterion was applied to extend the valid velocity points at the front

(backwards in time for each swash event) that were being erroneously excluded when only the water-depth criterion was considered. The chosen cutoff values were a minimum Corr of 70% (Puleo *et al.*, 2012) and a minimum SNR of 20 (Aagaard and Hughes, 2006).

The Corr and SNR criterion was not considered appropriate for extending the valid points in the end of the backwashes, as both varied significantly between values above and below the defined cutoff threshold during this offshore part of the events. Even though, the water-depth criterion was still allowing part of the backwash velocities not to be considered, thus biasing parameters such as the velocity skewness and asymmetry and the mean discharge.

Hence, another criterion was applied to extend the number of valid measured points in the end of each swash event. The values of velocity that had been excluded by the water-depth criterion, but which were measured for water depths greater than 1 mm, were replaced by a mean value obtained from the mean of the last 25 valid points (corresponding to a mean of the last *a.c.*0.19 s of measurement), and considered at the end of the backwash. **Erreur ! Source du renvoi introuvable.** shows an example of the application of the method described to a swash time series.

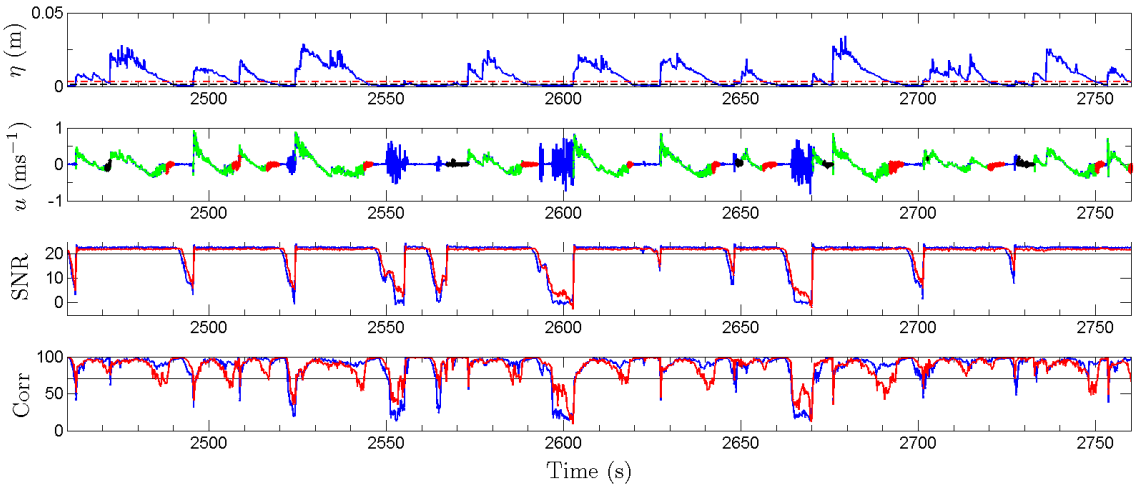

Figure 3. Example of the results obtained by the method for selecting swash events for x = 85.39 m, for condition A2. In free-surface plot: red dashed-dotted line represents water-depth limit, black dashed line represents 0.001-m limit. In the velocity plot: the blue full-line is the initial time series before the method was applied, the green line are the points considered valid after applying the water-depth criterion, the black points are the points added by considering the Corr and SNR criterion and the red points are the points added by the extrapolation of the mean of the last 25 values of the backwash. For both SNR and Corr plots, the blue/red lines correspond to the signal from beams 1/2, respectively, and the black lines set the thresholds of Corr = 70% and SNR = 20.

After processing all the data corresponding to measurements obtained with the ADV (which included both swash and surf zone time series), the percentage of submergence was computed for each position relative to the breakpoint for all the three A conditions, as well as the overall net discharge and both offshore and onshore net discharges. This allowed the identification of three distinct regions in the swash zone, where different processes are expected to dominate (Aagaard and Hughes, 2006).

Figure 4 shows a close-up on the inner surf/swash region of the domain and offers a greater insight on the mean velocities and wave set-up. The wave set-up is clearly greater for condition A2 (larger waves than A1 and A3); in this case, all measurement positions were below mean water level. For the highest water level all measurement positions were submerged, while for minimum water level, this happened only for two positions. For positions above/below the still water level, velocity tends to be directed onshore/offshore, respectively. Further offshore, in the inner-surf zone, the mean velocities measured at different elevations for the same cross-shore position are similar.

3.3 Decomposition of cross-shore velocity moments

The energetics approach (*e.g. Bagnold, 1963; Bowen, 1980; Bailard, 1981)* is one of the most robust sediment transport formulations for surf-zone conditions. According to this approach, the time averaged bed-load and a suspended-load are proportional to four velocity moments: the process-related moments $\langle |u|^2 u \rangle$ and $\langle |u|^3 u \rangle$, and the moments related to the gravity terms $\langle |u|^3 \rangle$ and $\langle |u|^5 \rangle$. Therefore, the

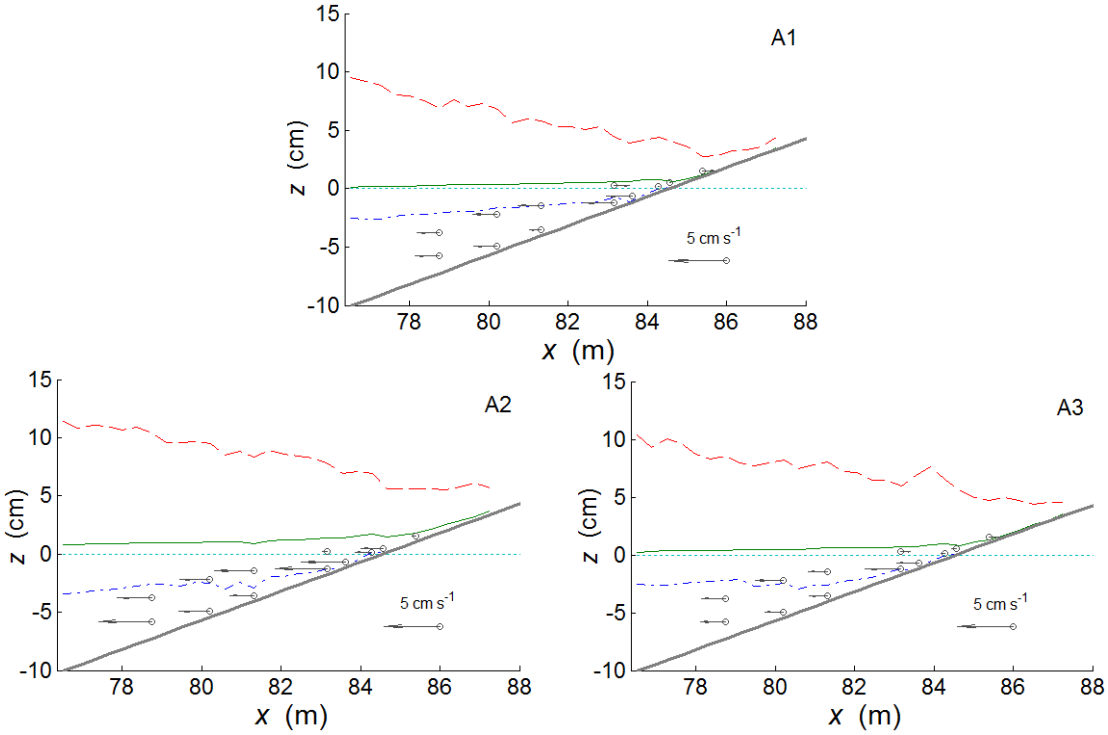

cross-shore structure of each velocity moment can help better understanding some of the different processes influencing sediment transport. Guza and Thornton (1985) have shown that the most important terms in the cross-shore transport equation are those included in the third and fourth velocity moments, $\langle |u|^2 u \rangle$ and $\langle |u|^3 u \rangle$, respectively. Russell and Huntley (1999) presented a detailed analysis to examine the relative contributions of incident waves, long period motions and mean flows and interactions between the three to the total structure of the moments using the normalized third velocity moment. This moment was chosen for having a clearer cross-shore structure, being statistically more robust, and its expansion into individual terms being easily coupled with well-known sediment transport mechanisms.

Figure 4. Close-up on inner-surf and swash zones. The arrows represent the mean velocity at each ADV measurement position, and the lines represent maximum (red dashed), mean (green solid), minimum (dashed-dotted blue) and still (dotted cyan) water elevation.

In order to study the relative importance of short and long waves on nonlinearity effects, the instantaneous near-bed cross-shore velocities can be split into a mean velocity ($\bar{u}$) term and an oscillatory ($\tilde{u}$) term. The latter can be further separated into high and low frequency components, corresponding to the short ($\tilde{u}_{HF}$) and long ($\tilde{u}_{LF}$) waves (1).

$$\boldsymbol{u = \bar{u} + \tilde{u}_{HF} + \tilde{u}_{LF}} \quad (1)$$

The third-order velocity moment, can then be computed resulting its decomposition in ten terms which can be related to different hydrodynamic processes:

Sk0:	$\bar{u}^3$	mean velocity cubed;
Sk1:	$\langle u_{HF}^3 \rangle$	skewness of short waves;
Sk2:	$3\langle u_{HF}^2 u_{LF} \rangle$	correlation of short-wave variance and long-wave velocity;
Sk3:	$3\langle u_{LF}^2 u_{HF} \rangle$	correlation of long-wave variance and short-wave velocity;
Sk4:	$\langle u_{LF}^3 \rangle$	skewness of long waves;
Sk5:	$3\langle u_{HF}^2 \rangle \bar{u}$	stirring by short waves and transport by mean flow;
Sk6:	$3\langle u_{LF}^2 \rangle \bar{u}$	stirring by long waves and transport by mean flow;
Sk7:	$6\langle u_{HF} u_{LF} \rangle \bar{u}$	three way correlation;
Sk8:	$3\langle u_{HF}^2 \rangle \bar{u}^2$	time-average of short-wave oscillatory component;
Sk9:	$3\langle u_{LF}^2 \rangle \bar{u}^2$	time-average of long-wave oscillatory component.

Each term was normalized by the velocity variance (wave energy), following Wells (1967), Bailard and Inman (1981) and Doering and Bowen (1987), enabling comparison of data collected under different energy conditions (Russell and Huntley, 1999).

3.4 Breakpoint position

The surf-zone width is a natural scaling factor for the velocity moments, as the wave-induced radiation stress, which drives the most important surf-zone dynamics, can be considered negligible outside this zone. Furthermore, it has already been recognized that cross-shore velocity moments have a consistent structure that depends on the position relative to the breakpoint.

Due to the very dissipative nature of the beach considered, wave breaking for random wave conditions was verified to occur over a large region of the domain, and thus definition of breakpoint position based on the maximum wave height was not accurate enough. Therefore, the energy-dissipation maximum was used instead, in order to define the breakpoint.

The energy balance is computed according to (2):

$$\frac{\partial (E C_g)}{\partial x} = -\langle \epsilon \rangle = -\left[\langle \epsilon_b \rangle + \langle \epsilon_f \rangle\right] \quad (2)$$

where E is the energy density, C_g is the group velocity ($= \sqrt{gh}$, in shallow water), $\langle \epsilon_b \rangle$ is the dissipation by breaking per unit area, and $\langle \epsilon_b \rangle$ is the frictional dissipation, which is considered negligible when compared with the dominant wave breaking dissipation. Assuming that the linear theory applies both in the shoaling and surf zones, E is computed as:

$$E = \frac{1}{8} \rho g H_{rms}^2 \quad (3)$$

Figure 5a shows the energy dissipation along the beach profile for each of the three random wave conditions. For all conditions there is a peak of energy dissipation, which occurs further from the shore for condition A2, the most energetic, and almost at the same position for both A1 and A3.

The definition of cross-shore position by means of water depth relative to breakpoint (h/h_b), allows a an improved separation of the different hydrodynamic zones of the profile and also a better comparison between the different random wave conditions. Figure 5b and Figure 5c present, as an example, the mean velocity and the wave set-up, respectively, plotted against the normalized depth, h/h_b. As expected, there is a significant increase of the mean offshore-directed velocity after the breakpoint, which continues to increase just to the very end of the surf zone. This offshore near-bed mean flow, the undertow, compensates the momentum flux induced by the roller towards the shore. Then, from the end of the surf zone, mean velocity becomes positive until the upper swash. It is also visible the wave set-down in the shoaling zone, which progressively changes to set-up after the breakpoint, reaching its maximum at the coast.

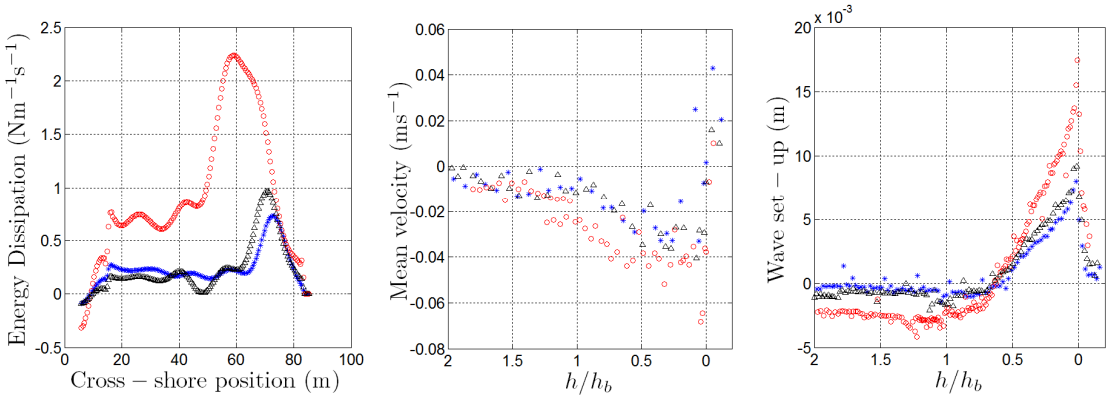

Figure 5. a) Energy dissipation rate, b) mean velocity and c) wave set-up along the beach profile, for A conditions (A1 – blue stars; A2 – red circles; A3 – black triangles).

4. Results

Root-mean-square wave height plots offer an overview of wave height evolution along the profile (Figure 6). A marked wave-height decrease in high frequencies, associated to breaking, is evident and is also associated with a notorious increase of long-waves wave height, which then dissipate very little energy as they progress almost to the shoreline. At the transition from surf to swash, the height of these low-frequency waves significantly decreases, an indication that these waves are dissipating their energy.

Following H_{rms} trends, the u_{rms} increases until slightly after the breakpoint, from where it decreases until close to the transition from surf to swash. Here, the velocity of the high-frequency component attains very-low values and there is a pronounced increase of the long-wave component, which reaches maxima values just before the swash zone, as the surf roller transfers its energy to the swash bore that then propagates up the beach. Afterwards, as the bore propagates higher up in the beach, velocity gradually diminishes.

The slight "bump" in H_{rms} values observed just before the shoreline, which is associated with the great increase of velocity just in the beginning of swash, may be explained by the changing from surf-zone roller to swash-zone bore, so the water piles up slightly as several consecutive waves catch each other to form the bores.

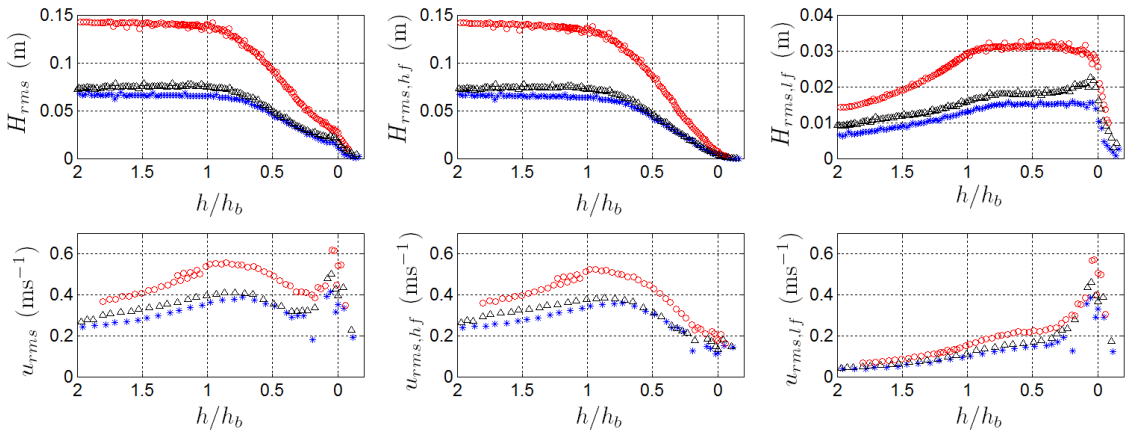

Figure 6. Root-mean-square wave height (top) and root-mean-square velocity (bottom) for all frequencies (left), high-frequencies (middle) and low-frequencies (right) for all A conditions, along the cross-shore profile (A1 – blue stars; A2 – red circles; A3 – black triangles).

Figure 7 shows the velocity-skewness distribution along the cross-shore profile ($Sk_u = \frac{\langle u^3 \rangle}{\sigma_u^3}$).

Overall skewness is negative offshore of the breakpoint for A1 and A2, while for the more narrow-banded condition, A3, it has slightly positive values until half the breakpoint depth, from where, together with A1 and A2 skewness, it assumes negative values until the transition from surf to swash. At

this point, the maximum negative skewness is observed, changing fast to very positive values in the middle- and upper-swash zones. It is also interesting to remark that the skewness evolution along the beach obtained for free surface, follows a very similar trend to that of the velocity skewness, even if it assumes greater values.

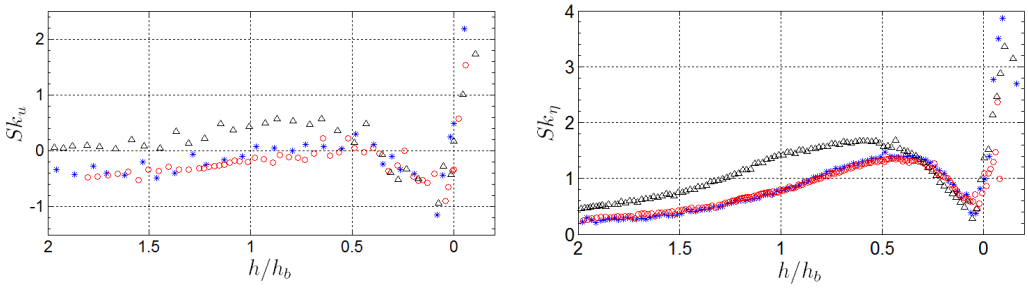

Figure 7. Velocity (left) and free surface (right) skewness (A1 – blue stars; A2 – red circles; A3 – black triangles).

The decomposition of the third-order velocity moment allows the analysis of the contribution of the different hydrodynamic processes to the total skewness. Hence, Figure 8 presents the distribution of the most relevant terms along the cross-shore profile (Sk1-6). The contribution of the other four terms, Sk0 and Sk7-9, was found to be less important (by at least one order of magnitude) and is not considered for analysis.

On the shoaling zone, the dominant term is the short-wave skewness, although there is also a contribution from the term corresponding to the stirring by shortwaves and transport by mean flow (see Figure 5b). Further, the the correlation between short-wave variance and long-wave velocity shows negative values: under non-breaking conditions the largest short waves appear under the bound long-wave trough (see Figure 1).

After the breakpoint and to the end of the surf zone, short-wave skewness continues to be positive. The stirring by short waves and transport by mean flow term contributes to negative skewness, with the most negative value at about half the breaking depth. Correlation of short-wave variance and long-wave velocity gradually becomes zero and then even becomes slightly positive between the breakpoint and the shoreline, as expected in a saturated surf zone where depth controls over height.

From the inner-surf to the upper-swash zone, the low-frequency waves start to clearly dominate the hydrodynamics. Long-wave stirring and transport by mean flow becomes increasingly more negative until close to the shoreline (Sk6). At the transition from surf to swash, with the formation of long-wave bores which propagate towards the upper-swash zone, the skewness of low-frequency waves becomes positive (Sk4) and a weak onshore-directed mean-flow effect is also present (Sk6). As short waves move associated with the long-wave bores, correlation of short-wave variance and long-wave velocity (Sk2) reaches greater and significantly-positive values. A small contribution from low-frequency wave variance correlation with high-frequency wave velocity also plays a role in the swash zone (Sk3).

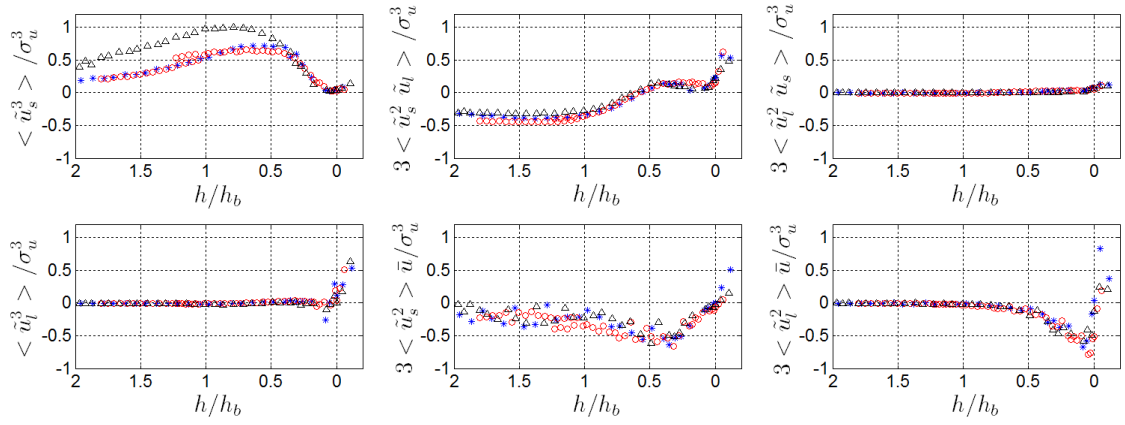

Figure 8. Terms Sk1-6 of the third-order velocity moment, normalized by the velocity variance (A1 – blue stars; A2 – red circles; A3 – black triangles).

Figure 9 shows the asymmetry trend along the profile, for both short and long waves ($Asy_u = \frac{\langle \mathcal{H}(u)^3 \rangle}{\sigma_u^3}$, where $\mathcal{H}$ represents the imaginary part of the Hilbert transform). The velocity-asymmetry of short waves presents positive values and becomes progressively more important between the breakpoint and the shoreline. The low-frequency component contributes with negative asymmetry seaward of the breakpoint, which becomes progressively positive inside the surf zone, reaching the greatest values near the transition from surf to swash, diminishing from there, as the bores dissipate up the beach.

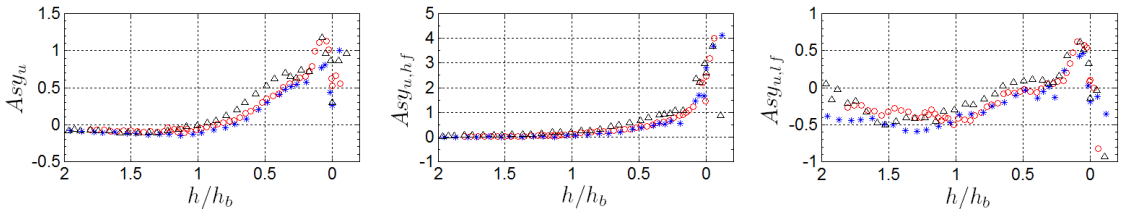

Figure 9. Velocity asymmetry for all frequencies (left), high frequencies (middle) and low frequencies (right) (A1 – blue stars; A2 – red circles; A3 – black triangles).

5. Discussion and Conclusions

The results obtained herein are in agreement with the hydrodynamics expected on dissipative beaches, with short-wave energy saturation in the surf zone and long-wave dominance on the inner-surf and swash zones. In this very-low sloping beach, also long waves change their shape, which generates velocity skewness and asymmetry effects, and eventually breaking, in the swash zone.

A strong dependency of hydrodynamic processes on distance to breakpoint was found, with markedly different behaviours offshore and onshore of the breaking position. There is already accumulated evidence that suggests that the magnitude and direction of the sediment transport also depend on the cross-shore location relative to the breaking point. Several studies have shown that seaward of the surf zone (under nonbreaking wave conditions) onshore transport promoted by short-wave skewness tends to dominate (Guza and Thornton, 1985; Roelvink and Stive, 1989; Beach and Sternberg, 1991; Osborne and Greenwood, 1992; Doering and Bowen, 1995; Russell and Huntley, 1999), even if an offshore transport induced by bound long waves is present (Ruessink *et al.*, 1998; Russell and Huntley, 1999). Inside the surf zone, wave breaking generates mean flows, such as the undertow, and energy transfers to lower and higher frequencies that modify wave characteristics, and thus deeply affect sediment transport, which tends to be offshore directed (Mariño-Tapia *et al.*, 2007). In the swash zone, onshore transport is expected both in low and high-energy wave conditions (Tinker *et al.*, 2009).

The present results show that short-wave skewness (Sk1), short-wave variance correlation to long-wave velocity (Sk2) and stirring by short-waves and transport by mean flow (Sk5) are the dominant terms outside the surf zone. This is in accordance with the findings of Russell and Huntley (1999) and Mariño-Tapia *et al.* (2007), who also observed the terms Sk1 and Sk2 to be positive and negative, respectively, offshore of the breakpoint. However, the positive values perceived by these authors for the term Sk5 were not found herein, where undertow has a stronger signature, leading to negative values. This leads to a distinct behaviour of the overall velocity skewness when compared with the shape function of Mariño-Tapia *et al.* (2007).

Again inside the surf zone, the results obtained are in agreement with previous findings, with a predominance of negative skewness, although this is only strictly true for depths shallower than half the breakpoint depth, where the mean velocity reaches more negative values and the wave set-up builds up. Terms Sk5 and Sk6 are the largest, representing the stirring by both short and long waves, and subsequent transport offshore by the mean flow. Between these two terms, it is the stirring by long waves that assumes the greatest importance in the inner-surf zone. Short waves are still skewed onshore, with skewness peaking also at about half the breakpoint depth from where it decreases to much-smaller values. Further relevant changes occur at the end of the surf zone and the beginning of the swash, as the surf-zone rollers transform into swash-zone bores. Additionally, it is from the inner-surf zone that the importance of long waves becomes notorious and extends into the swash zone. In this zone, long waves clearly dominate the velocity field (Figure 6). The correlation between short-wave variance and long-wave velocity is significantly positive as the largest short waves only propagate at long-wave crests, and the skewness of long waves and the stirring by long waves and transport by mean flow are the most important

terms, and are both positive. There are also minor contributions from the terms Sk3 and Sk5. Overall, in the swash zone, all the terms contribute to positive skewness, which would promote onshore transport in the swash zone for the simulated wave conditions.

However, it is important to stress that the velocity-moments approach ignores the contribution of fluid acceleration on sediment transport processes (Silva *et al.*, 2011). The presence of positive values of velocity asymmetry for the short-wave component and negative values for the long-wave component suggest a more complex picture.

Skewness and asymmetry in the swash zone have just recently started to be studied, both because quality swash data are hard to retrieve and, mostly, because non-continuous velocity time series are difficult to analyze. Particularly regarding the frequency-domain filtering that is applied to separate high and low frequencies, some questions persist. For the shoaling and surf zones, no greater issues come from considering a separation between high and low frequencies at half the peak frequency. Frequencies higher than this threshold are supposed to correspond to the short waves, and lower frequencies to both long-waves and mean-flow components. However, when the swash zone is considered, some concerns can be raised.

As the beach considered herein is a very low-sloping one, besides the importance of the long waves in the swash zone, there is also the fact that the nonlinearities of both short and long waves have time to develop as the waves propagate along the cross-shore profile. Hence, even the long waves become skewed and asymmetric before breaking. These skewed/asymmetric long waves are a sum of the fundamental frequency and the higher harmonics that gradually receive energy from the lower frequencies. Therefore, at a given point in the swash, filtering the velocity signal in the frequency domain will lead to considering part of the actual long waves (their subharmonics) as short waves (high frequencies). The result is that the low-frequency part of the signal does not represent the real nonlinear long waves that exist in the swash, but instead it only accounts for the low-frequency fundamental component. If this is considered together with the fact that the separation of the swash events, especially for the positions in the middle and upper swash, is a challenging task and involves the application of methods far from being perfect, it should be borne in mind that the results obtained in the swash zone are to be subjected to further analysis and more work on this topic is necessary to validate the results obtained herein.

6. Acknowledgments

This work was supported by the grant conceded to the Integrated Infrastructure Initiative Hydralab IV, Contract no. 261520, by the European Community's Seventh Framework Programme and by FCT (Portuguese Science and Technology Foundation) grant SFRH/BD/80644/2011.

7. References

Aagaard, T. and Hughes, M. G. (2006). Sediment suspension and turbulence in the swash zone of dissipative beaches. *Marine Geology*, 228: 117-135.

Alsina, J. M. and Cáceres, I. (2011). Sediment suspension events in the inner surf and swash zone. Measurements in large-scale and high-energy wave conditions. *Coastal Engineering*, 58(8): 657-670.

Bailard, J. A. (1981). An energetics total load sediment transport model for a plane sloping beach. *Journal of Geophysical Research: Ocean*s, 86(C11): 10938-10954.

Bailard, J. A. and Inman, D. L. (1981). An energetics bedload model for a plane sloping beach: Local transport. *Journal of Geophysical Research: Oceans*, 86(C3): 2035-2043.

Baldock, T. E., Alsina, J. A., Caceres, I., Vicinanza, D., Contestabile, P., Power, H. and Sanchez-Arcilla, A. (2011). Large-scale experiments on beach profile evolution and surf and swash zone sediment transport induced by long waves, wave groups and random waves. Coastal Engineering, 58: 214-227.

Beach, R. A. and Sternberg, R. W. (1991). Infragravity driven suspended sediment transport in the swash, inner and outer-surf zone. *Coastal Sediments*, ASCE, New York.

Cáceres, I. and Alsina, J. M. (2012). A detailed, event-by-event analysis of suspended sediment concentration in the swash zone. *Continental Shelf Research* 41: 61-76.

De Bakker, A., Tissier, M., Marieu, V., Sénéchal, N., Ruju, A., Lara, J., Ruessink, B.G. (2013). Infragravity wave propagation and dissipation on a low-sloping laboratory beach. *Proc. Coastal Dynamics.*

Didenkulova, I. and Soomere, T. (2011). Formation of two-section cross-shore profile under joint influence of

random short waves and groups of long waves. Marine Geology, 289: 29-33.

Doering, J. C. and Bowen, A. J. (1987). Skewness in the nearshore zone: A comparison of estimates from Marsh-McBirney current meters and colocated pressure sensors. *Journal of Geophysical Research: Oceans*, 92(C12): 13173-13183.

Doering, J. C. and Bowen, A. J. (1995). Parametrization of orbital velocity asymmetries of shoaling and breaking waves using bispectral analysis. *Coastal Engineering*, 26(1–2): 15-33.

Elgar, S. and Guza, R. T. (1985). Observations of bispectra of shoaling surface gravity waves. Journal of Fluid Mechanics, 161: 425-448.

Guza, R. T. and Thornton, E. (1985). Velocity moments in nearshore. *J. of Waterway, Port Coast. Ocean Eng.*, 111(2): 235-256.

Mariño-Tapia, I. J., Russell, P. E., O'Hare, T. J., Davidson, M. A. and Huntley, D. A. (2007). Cross-shore sediment transport on natural beaches and its relation to sandbar migration patterns: 1. Field observations and derivation of a transport parameterization. *Journal of Geophysical Research*, 112 C03001.

Michallet, H., Cienfuegos, R., Barthélemy, E. and Grasso, F. (2011). Kinematics of waves propagating and breaking on a barred beach. *European Journal of Mechanics B/Fluids*, 30(6): 624-634.

Mori, N., Suzuki, T. and Kakuno, S. (2007). Noise of Acoustic Doppler Velocimeter Data in Bubbly Flows. *Journal of Engineering Mechanics*, 133(1): 122-125.

Osborne, P. D. and Greenwood, B. (1992). Frequency dependent cross-shore suspended sediment transport. 2. A barred shoreface. *Marine Geology*, 106: 25-51.

Puleo, J. A., Lanckriet, T. and Wang, P. (2012). Near bed cross-shore velocity profiles, bed shear stress and friction on the foreshore of a microtidal beach. *Coastal Engineering*, 68(0): 6-16.

Roelvink, J. A. and Stive, M. J. F. (1989). Bar-generating cross-shore flow mechanisms on a beach. *Journal of Geophysical Research*, 94(C4): 4785-4800.

Ruessink, B. G., Kleinhans, M. G. and van den Beukel, P. G. L. (1998). Observations of swash under highly dissipative conditions. *Journal Geophysical Research*, 103: 3111-3118.

Ruessink, B. G., Michallet, H., Abreu, T., Sancho, F., Van der A, D. A., Van der Werf, J. J. and Silva, P. A. (2011). Observations of velocities, sand concentrations, and fluxes under velocity-asymmetric oscillatory flows. J. Geophys. Res., 116(C3): C03004.

Ruessink, B.G., Michallet, H., Bonneton, P., Mouazé, D., Lara, J., Silva, P.A., Wellens, P. (2013). GLOBEX : Wave dynamics on a gently sloping laboratory beach. *Proc. Coastal Dynamics.*

Russell, P. E. and Huntley, D. A. (1999). A Cross-Shore Transport "Shape Function" for High Energy Beaches. *Journal of Coastal Research*, 15(1): 198-205.

Silva, P. A., Abreu, T., van der A, D. A., Sancho, F., Ruessink, B. G., van der Werf, J. and J.S., R. (2011). Sediment transport in nonlinear skewed oscillatory flows: Transkew experiments. *Journal of Hydraulic Research*, 49(1): 72-80.

Tinker, J., O'Hare, T., Masselink, G., Butt, T. and Russell, P. (2009). A cross-shore suspended sediment transport shape function parameterisation for natural beaches. *Continental Shelf Research*, 29(16): 1948-1960.

Van der A., D.A., Mouazé, D., Vignal, L., Silva, P.A., Abreu, T., Barthélemy, E. and Michallet, H. (2013). Wave boundary layer dynamics on a low sloping laboratory beach. *Proc. Coastal Dynamics.*

van Dongeren, A., Battjes, J., Janssen, T., van Noorloos, J., Steenhauer, K., Steenbergen, G. and Reniers, A. (2007). Shoaling and shoreline dissipation of low-frequency waves. *Journal of Geophysical Research*, 112: C02011.

Voulgaris, G. and Trowbridge, J. H. (1998). Evaluation of the Acoustic Doppler Velocimeter (ADV) for Turbulence Measurements. Journal of Atmospheric and Oceanic Technology, 15(1): 272-289.

Wells, D. R. (1967). Beach equilibrium and second-order wave theory. *Journal of Geophysical Research*, 72(2): 497-504.